Observation of heat wave effects on the urban air quality and PBL in New York City area

Yonghua Wu [1*], Kaihu Zhao [1, 2], Jianping Huang [3], Mark Arend [1], Barry Gross [1], Fred Moshary [1]

[1] NOAA-CREST at the City College of New York, New York, NY 10031, USA *Email: yhwu@ccny.cuny.edu

[2] School of Environment and Energy, South China University of Technology, Guangzhou, China

[3] NOAA-NCEP Environmental Modeling Center (EMC) and IM System Group Inc., College Park, MD 20740, USA

Abstract: Heat waves are of serious health concern in highly populated urban areas due to combined heat stress and poor air quality impacts. In this study, we present an observation-based study of the heat-wave impacts on the planetary-boundary-layer (PBL) and air quality in summer 2017 in New York City (NYC). Synergy of remote sensing, in-situ observations with model forecast is applied to quantify and characterize the diurnal variation of PBL height (PBLH), ozone (O_3) and $PM_{2.5}$ during the heat wave period of June 11-13, 2017. The ground O_3 concentration attains a maximum of 110 ppb largely exceeding the U.S. National Ambient Air Quality Standard (NAAQS) while the organic carbon (OC) and sulfate aerosols show a coincident increase. The higher O_3 in the downwind suburb than those in the urban area are likely associated with the urban pollution transport and local meteorological condition. We observe a dramatic and consistent PBLH growth from 0.5- to 2.5-km at 11:00-13:00 local time from the turbulence-based and aerosol-based PBLH estimate by co-located ceilometer, wind lidar, and aerosol lidar measurement. Regional and high residual layers of aerosols at night are observed from the NASA space-borne Cloud-Aerosol Lidar with Orthogonal Polarization (CALIOP) and Cloud and Aerosol Transport System (CATS) lidars. Furthermore, we evaluate the NOAA National Air Quality Forecasting Capability (NAQFC) products of PBLH, temperature, O_3, $PM_{2.5}$ and NOx (NO_2+NO) with the observations. Under the strong convective PBL condition, all the products above show good agreement between the NAQFC predictions and observations. However, in the early morning and night, the model shows dramatic discrepancies with an underestimate of temperature, PBLH and O_3 but an overestimate of $PM_{2.5}$ and NOx. Such bias may be associated with the improper representations of vertical mixing, complex chemical processes and emissions in the model.

Key words: Heat wave, air pollution, lidar, model, remote sensing

1. Introduction

Intensity, frequency, and duration of heat waves are expected to increase as a consequence of climate change, which make important reprecuations for human and ecosystems health (Horton et al. 2016; Meehl, 2004; Lau et al., 2012; Schnell et al., 2017). The irregular nature of heat waves, including variations manifested in frequency, magnitude, duration and areal extent has led to a lack of consistency in their definition (Meehl and Tebaldi 2004). In the United States (US), definitions also vary by region. In the northeast US, a heat wave is typically defined as three consecutive days where the temperature reaches or exceeds 90 °F (32.2 °C) (Robinson et al., 2001); this study follows the definition above.

Heat waves form when a high-pressure system develops and remains over a region for several days, which is often accompanied with large-scale subsidence and leads to clear skies and weak winds, and substantially suppresses air pollutant dispersion. During the heat-wave period, elevated temperatures, strong sunlight, low wind speeds, and anthropogenic emissions allow heat and poor air quality to stagnate in a given location for an extended period of time (Tressol et al., 2007). For instance, the combination of strong sunlight with nitrogen oxide (NOx), volatile organic compounds (VOCs), and sulfur dioxide (SO_2) emissions from motor vehicles and industry can create a cocktail of unhealthy pollutants, in particular resulting in the O_3 exceedance of NAAQS. Schnell and Prather (2017) showed the concurrence of heat waves and air pollution in the eastern United States and Canada. Hou et al. (2016) found that in the US the probability of severe ozone pollution when there are heat waves could be up to seven times of the average probability. Though O_3 concentration usually increases with temperature in summer, Shen et al. (2016) found that 20 percent of measurement sites in the US show O_3 suppression at extremely high temperatures beginning in the mid-90s Fahrenheit; and they suggested that this reduction of O_3 level was caused by meteorological process. Haman et al (2014) investigated the relationship between PBL heights with ground O_3 in Houston, and found that night and early morning observed and modeled PBL heights are consistently lower on high-O_3 days than on low-O_3 days. In addition, on hot and humid days, more or abundant fine particulate matter (i.e. $PM_{2.5}$ particulate matter with diameter less than 2.5 micrometers) can be produced

through photochemical oxidation reactions, which is generally referred to as secondary inorganic species (e.g. sulfate, nitrate, ammonium) and secondary organic aerosols (SOAs). However, because of the complex nature of organic material in air, much is still to be learned about the sources, formation, and even spatial and temporal distributions of the SOAs (Fine et al., 2008). In addition, increased temperatures and solar radiation favor biogenic emissions of isoprene with a potential for enhanced ozone chemistry in the PBL (Lee et al., 2006). Thus, heat waves and air pollutions are synergistic stressors that produce disproportionately greater adverse health impacts.

On the other hand, heat wave can aggravate the Urban Heat Island (UHI) effect in the urban area; and the greater temperatures of the UHI lead to more emissions and faster pollutant production and overwhelm the effects of dilution (EPA 2006). The observation and model studies indicate strong interactions between heat waves and UHI in NYC area (Li et al., 2013; Ramamurthy et al., 2017, Zhao et al., 2018). The UHI intensity was nearly twice compared to the decadal average and thus affecting the PBL thermal structure and wind fields during July 2016 (Ramamurthy et al., 2017). Gutiérrez and González (2015) found that the multilayer Building Energy Parameterization (BEP) coupled with the Building Energy Model (BEM) in the urban-WRF model showed dramatic influences on the profiles of temperature, wind and turbulent kinetic energy (TKE) in the urban canopy during a heat-wave event. Ortiz et al (2018) assessed the impacts of an urban surface, urban canopy, and a synoptic heatwave condition on the UHI, potential temperature and wind vertical profile for 4–8 July 2010 heat wave in NYC. Their results indicate the nonlinear interactions between the urban surface and heat wave magnified the nighttime UHI by up to 6 ˚C in the urban areas. Zhang (2011) simulated the impact of upstream urbanization on the UHI along the Washington–Baltimore Corridor, and indicated that without the upstream urbanization, the UHI effects over Baltimore would be 1.25 ˚C weaker with a 200-m shallower mixed PBL and then may affect surface O_3 concentration.

Due to the need to forecast such extremely hot events and issue warnings to vulnerable populations in urban areas, accurate weather forecast and air quality models that can quantify the effects of these events are needed. However, complex urban emission sources, canopy and energy use make the modeling difficult

in hot weather. Zhang et al. (2012) indicated that the parameterizations for urban sublayer process and physiographic data are challenging but critically important for the $PM_{2.5}$ forecast in the urban areas since they effect pollutant turbulent mixing, dispersion and deposition. Hu et al (2013) showed that the differences among the WRF-PBL schemes are predominantly due to differences in vertical mixing strength and entrainment of air from above the PBL. Yegorova et al. (2011) showed that the WRF/Chem under-predicted O_3 maxima by 5–8 ppb in the northeast US, but over-predicted maxima by up to 16 ppb where ozone amounts were low in the southeast. Such biases were closely associated with the complexity of photochemical processes, uncertainties in O_3 precursors (e.g., NOx) emissions, vertical mixing and/or O_3 titration by NO. Zhao et al (2019) evaluated the ozone product of WRF/Chem model during a heat-wave event in NYC areas, and indicated the VOCs influences on the O_3 production in NYC area. On the other hand, Hogrefe et al (2007) show that total $PM_{2.5}$ mass was strongly overestimated in the NYC metropolitan areas; and most of the over-prediction stems from organic aerosols and crustal material. Doraiswamy et al. (2010) demonstrated that the CMAQ model significantly over-predicted $PM_{2.5}$ in NYC both in the pre-morning and post-sunset hours. Briefly, mechanisms for near-surface ozone formation and depletion are complex in urban areas, which are associated with vertical and horizontal advection, complex emissions of O_3 precursors (NOx, VOCs, CO) and chemical processes, dry and wet deposition, etc. For these reasons, air quality forecast over urban areas under heat-wave conditions is challenging.

New York City (40.821ºN/73.95ºW) is at the heart of the largest urban region in US with heavy traffic due to dense population along the northeast US. It is vulnerable to heat waves due to high electrical energy consumption for cooling and air quality related to the motor vehicles emissions. The combined effects of heat wave and UHI make the impact on air quality even larger. However, there are few studies in the literatures that quantify heat-wave impacts on both the air quality and PBL height in NYC and its surroundings. In addition, the mechanism of urban pollution transport and influences on the adjacent downwind coastal areas require an in depth analysis of the surface and profiling observations, particularly the vertical distribution and structures of meteorological, aerosol and ozone (Miller, 2017). Yet, the

105 Community Multiscale Air Quality (CMAQ) model performance for air quality forecasts during the
106 heatwave days in the NYC areas is not well evaluated.

107 The goals of this study are to quantify the heat-wave effects on the PBLH and air quality, and
108 evaluate the model forecast capability using synergistic remote sensing, in-situ and satellite measurement
109 in NYC and surrounding areas. We present the observation-based diurnal variations of PBLH, ground $PM_{2.5}$
110 and its compositions (OC, elemental carbon (EC), sulfate, etc.), O_3 and its precursors during a heat-wave
111 event in June 2017. In particular, co-located ceilometer, wind lidar and aerosol lidar measurements provide
112 high spatial-temporal distribution of aerosols, PBL and residual-layer heights, turbulence intensity and
113 cloud formation. Regional nocturnal PBLH is derived from the NASA satellite-borne lidars (CALISPO and
114 CATS) around the NYC coastal areas. The temporal and spatial variability of $PM_{2.5}$, O_3 and NOx is
115 investigated at the urban and suburb sites. Finally, we utilize the observation data to evaluate the NOAA
116 NAQFC model forecast of air quality. The paper is organized as follows. Section 2 gives the observation
117 methodology and data; Section 3 shows the results and discussions, and Section 4 gives the conclusion.

118 ## 2. Observation Methodology and Data

119 ### 2.1 Ground-based observation

120 A suite of ground-based remote sensing instruments is deployed on a building rooftop at CCNY. The
121 instruments include a ceilometer, a 3-wavelength elastic-Raman lidar, an AERONET Cimel sun/sky
122 radiometer, and a coherent Doppler wind lidar. Meanwhile, a standard surface air quality monitoring station
123 is operated on the CCNY campus by the New York State Department of Environment Conservation
124 (NYSDEC) and makes hourly $PM_{2.5}$, O_3 and CO measurements. There is another AERONET site (LISCO
125 40.955º N, 73.3419º W) in the northeast of CCNY-site (54 km away) and a national weather service station
126 at Upton New York (OKX, 40.87º N, 72.86º W) with routine radiosonde launch for meteorological profiling
127 observation. Figure 1 gives the locations of some ground stations used in this study.

128 According to Stull (1988), a convective boundary layer (CBL) that occurs during the daytime is usually
129 referred to as a mixing layer. At the sunset, the surface cooling creates a stable (nocturnal) boundary layer,

above which is a residual layer, leftover from the daytime mixed layer. The ceilometer (Vaisala CL-51) measures laser backscatter at a wavelength of 910 nm with a range resolution of 10 m (Gan et al., 2011). It makes fully automatic 24-hr/7-day observations in all-weather conditions. It provides attenuated backscatter coefficient profile that can be used to determine PBLH and residual layer height, which allows monitoring of the PBL process and evolution for air pollution studies. Its co-axial configuration of transmitter and receiver makes it possible to measure at the near surface close to 30-m above the ground level (AGL) that can be used to estimate low-level PBLH at night and early morning. This is important to evaluate the modeling PBLH for the air quality applications, especially during nighttime or over water surface (like lakes or ocean). To reduce the inherent noise limitation, the raw data are smoothed with a time-range window of 3-min and 300-m. The PBLH can be detected from the ceilometer and lidar based on vertical gradient variation of aerosol backscatter. Several methods or techniques have been suggested, including the first derivative, maximum variance, curve-fitting threshold and wavelet transform methods (Menut et al., 1999; Cohn et al., 2000; Brooks, 2003; Haeffelin et al., 2012). The results generally show good consistency among these methods except the scenario with weak signal-to-noise ratio, aloft and residual aerosol layer (Wiegner et al, 2006, Haeffelin et al., 2012). In this study, a wavelet analysis technique is used to locate the absolute maximum negative gradient of attenuated backscatter profile that is defined as the PBLH (Gan et al., 2011). A quality control of the PBLH value is performed which includes cloud screening, temporal continuity, and screening of an aloft or residual layer in the night and mid-morning. In addition, the residual-layer-height is estimated from the second sharp gradient of aerosol profile in the early morning and night.

The CCNY-lidar transmits three wavelengths (1064-, 532- and 355-nm) with a flash lamp-pumped Nd: YAG laser at a repetition rate of 30 Hz (Spectra-physics Quanta-Ray PRO-320) (Wu et al., 2009). A receiver telescope (Ø50-cm) collects three elastic scattering and two Raman-scattering returns by nitrogen and water vapor molecules excited by 355-nm laser output. The signals are acquired and recorded with 1-min average and 3.75 m range resolution. The full return signals are detected starting at the initial altitude 0.5 km. It is generally operated in the daytime on weekdays with an observer due to the eye-safety concerns.

156 The multi-wavelength configuration can be used to obtain color-ratio or Angstrom exponent (AE) that help
157 discriminate fine mode (smoke and industrial aerosol) from the coarse mode particles (dust and cloud). The
158 strong signal-to-noise ratios (SNR) permit us to measure aloft aerosol plumes and retrieve aerosol extinction
159 and backscatter profiles in the troposphere. The PBLH is estimated from the lidar returns at 1064-nm with
160 a wavelet transform method because they are more sensitive to the aerosol structures than those at 355-nm
161 and 532-nm due to weaker molecular backscattering (Gan et al., 2011). By combining the lidar and
162 ceilometer returns, the retrieval of aerosol backscatter can be extended to the near surface. Thus, one can
163 obtain boundary layer information as well as residual-layer height, aerosol-cloud discrimination, and optical
164 properties of aerosols and clouds from the CCNY-lidar measurement (Wu et al., 2009, 2018). In addition,
165 two CIMEL sunphotometers (part of the NASA AERONET) at CCNY and LISCO provide column aerosol
166 optical depth (AOD), Angstrom exponent (AE), and microphysical parameters (volume size distribution
167 and refractive index and single-scattering albedo) (Holben et al., 1998).

168 A coherent Doppler lidar (Leosphere Windcube 200S) has been installed to measure wind profiles
169 at CCNY campus since spring 2017. It provides 24-hr/7-day wind measurements in the PBL under all
170 weather conditions**.** The lidar has a range-gate spacing of 25-50 m and time resolution of 1 second. The
171 intensity of the turbulence can be characterized by the variance of the vertical velocity *w* over an interval
172 of a few minutes (Hogan et al., 2009; Tucker et al., 2009). The turbulence-based PBLH can be calculated
173 from the variance of vertical velocity with a threshold method (e.g. 0.15 m/s^2 in this study) (Schween et al.,
174 2014). Thus, the co-located wind lidar, ceilometer and CCNY-lidar provide a unique opportunity to evaluate
175 the PBLH result from the turbulence- and aerosol-based methods.

176 New York State Department of Environment Conservation (NYSDEC) operates O_3, NO_x, $PM_{2.5}$
177 and $PM_{2.5}$ speciation (OC, EC, sulfate (SO_4^{2-}), nitrate (NO_3^-), ammonium (NH_4^+), and metal ions, etc.)
178 samplers at the urban, suburban and rural sites (Rattigan et al., 2010, 2016). The locations of ground stations
179 are shown in Fig.1. Co-located at CCNY campus, the $PM_{2.5}$, O_3 and CO are reported hourly. Queens College
180 (QC, 40.736º N/73.822º W in the borough of Queens) and IS-52 (located in borough of Bronx) are two
181 Chemical Speciation Network (CSN) trends sites in New York State, there is an extensive set of ambient

monitoring equipment for gaseous and aerosol sampling (e.g. O_3, NO_2, NO, SO_2, CO, $PM_{2.5}$ and its speciation). In addition, the sites at Riverhead, Babylon and Suffolk located in the eastern NYC may represent the downwind area of NYC with the prevailing western and southwest winds, where the hourly O_3 is observed. The site of Division Street (DivStr) is located in southern Manhattan, NYC. Two rural sites at Pinnacle State Park (42.09˚N,-77.21˚W, ~500 m ASL) and Whiteface Mountain (44.39˚N, -73.86˚W, ~1500m ASL) located in the northwest/north of NYC represent the rural or background sites since they are far from the city and with little local emissions (Rattigan et al., 2016). Further details about these sites can be found at the website (http://www.dec.ny.gov/chemical/8406.html).

Hourly OC, EC and sulfate of $PM_{2.5}$ are measured using a Sunset OC/EC field analyzer (Sunset Lab, Inc.) and sulfate particulate analyzer (SPA, Thermo Electron Company, model 5020), respectively (Rattigan et al., 2010). The minimum detection limit on the hourly OC and EC data is approximately 0.40 $\mu g/m^3$ (Bauer et al., 2009; Rattigan et al., 2010). Organic matter (OM) in the $PM_{2.5}$ can be estimated from the OC by multiplying a factor of 1.6 (Bae et al., 2006; Rattigan et al., 2016). Meanwhile, a two-wavelength aethalometer (Magee Scientific model AE-21, 880 nm and 370 nm) measures BC at the urban (IS-52) and rural (Pinnacle and Whiteface Mt.) sites (Rattigan et al., 2013). The BC measured at the two wavelengths, BCUV370 and BC880, can help distinguish the BC sources (e.g. vehicles vs. biomass burning) because of their differences from the organic absorption (BCUV370 > BC880) (Wang et al., 2012). In addition, the 24-hr integrated filter sampling measurements are carried once-every-3-day (1-in-3 day) following the planned schedule in the EPA Chemical Speciation Network (CSN) and Interagency Monitoring of Protected Visual Environments (IMPROVE). OC is generally emitted from combustion activities or produced from secondary processes such as gas-to-particle formation. EC, also known as light absorbing carbon or black carbon (BC), is emitted directly from combustion sources.

2.2 Satellite products

The NOAA Hazard Mapping System (HMS) was developed in 2001 by the National Environmental Satellite and Data Information Service (NESDIS) as an interactive tool to identify fires and smoke

emissions over North America in an operational environment (Ruminski et al., 2016). The system utilizes two geostationary and five polar orbiting environmental satellites (https://www.ospo.noaa.gov/Products/land/hms.html). The result is a quality-controlled display of the locations of fires and significant smoke plumes. HMS has a number of detection limitations such as clouds hindering detections, no vertical structure information and no quantitative amount or density of smokes and is only available during daylight. In addition, the NOAA- HYbrid Single Particle Lagrangian Integrated Trajectory (HYSPLIT) model is used to compute air parcel trajectories and model the dispersion and the route of airborne particles (Draxler et al., 1997) and can be used either in a back-trajectory mode to analyze sources or in forecast mode.

CALIOP instrument on board the CALIPSO satellite platform is a space-borne polarization-sensitive two-wavelength (532- and 1064-nm) lidar (Vaughan, et al., 2009). It observes global aerosol/cloud vertical distribution and provides aerosol type classification and optical properties products. CALIPSO has a narrow laser footprint (~70 m) at the earth's surface and a 16-day revisit cycle. The laser pulse repetition frequency of 20.16 Hz produces profile every 335 m along the ground. In this study, the latest release product (Version 4.10, Level-1 attenuated backscatters, linear volume depolarization ratio and Level-2 aerosol extinction and aerosol type classification) are used. In addition, the NASA's CATS is a lidar remote sensing instrument that provides range-resolved profile measurements of atmospheric aerosols and clouds from the International Space Station (ISS) from Feb. 2015 to Oct. 2017 (Yorks, et al., 2016). At present, the released CALIPSO and CATS aerosol products include (i) Level-1 attenuated backscatter coefficient profiles or calibrated range-corrected lidar returns; (ii) Level-2 aerosol and cloud layer product, vertical-feature-mask (VFM) including cloud-aerosol discrimination (CAD) and aerosol-type classification, extinction and backscatter coefficient profiles; (iii) Level-3 aerosol globally gridded monthly profile product. In this study, we calculate the regional PBLH along the satellite track with the Level-1 attenuated backscatter profile using a wavelet transform analysis. Finally, the routine radiosonde measurements at OKX near NYC are also used to show PBLH and structure; the vertical profiles include temperature, virtual

potential temperature, water vapor mixing ratio, wind velocity and direction at 00:00 and 12:00 UTC (local summer time 8:00 am and 8:00 pm).

2.3 NAQFC (the NOAA National Air Quality Forecasting Capability) model

NAQFC consists of the NOAA-NCEP regional operational weather forecasting model (NAM-North America Model) and EPA-CMAQ model (Lee et al., 2016; Huang et al., 2017). It is designed to provide 2-day model forecasts of O_3 and $PM_{2.5}$ twice per day at the 06 and 12 UTC cycles. For this study, products with spatial resolution of 12 km at the 06 UTC cycle are used. The NAQFC program performs incremental tests and evaluations against the U.S. EPA AIRNow surface monitoring network.

A modified version of the U. S. EPA CMAQ model (version 4.6) dubbed CMAQ v4.6.5 (Foley et al., 2010), is run with 12 km horizontal grid spacing with a Lambert Conformal Conic (LCC) map projection for the product used in this study. The offline coupling between NWS/NCEP NAM meteorological model and CMAQ is achieved by two pre-processors. In addition to the coupled NMMB-CMAQ system, there are other components such as the emission module and the chemical lateral boundary condition builder as well as the products generating post-processing components. Emission inventories are processed by sectors, but the fire sectors do not include prescribed burns and wildfires from the National Emission Inventory (NEI). The U.S. EPA-NEI 2011 version-1 is being incorporated into Premaq's emission projection schemes. The 2006 Environment Canada National Inventory sources were used for Canada, and the 2012 Mexico NEI non-road sources were used for Mexico. The emissions from wildfires, prescribed agricultural burns, and land clearing fires were computed using the dynamic fire emission modeling U.S. Forest Service BlueSky smoke emission package (O'Neill et al., 2009) and the NOAA-HMS for fire locations and strength.

The NAQFC CMAQv4.6.5 follows largely the U.S. EPA Aero4 module and the related emission and removal processes found in the U.S. EPA-CMAQ version 4.6. Gas to particle conversion, heterogeneous reactions, depositional growth, and coagulation are included (Kelly et al., 2009). The Aero4 module simulates particle formation, condensational and coagulation growth or evaporative dissipation of existing particles due to ambient chemical, temperature and humidity conditions. The Mellor Yamada Janjic

257 (MYJ) PBL scheme (Janjie et al., 2001) is used in this version of NAM. The detailed configuration for
258 NAM-CMAQ system can be found in Lee et al. (2016).

259 ## 3. Results and Discussions

260 ### 3.1 O_3 exceedance and $PM_{2.5}$ increment

261 The temporal variations of near-surface air temperature and wind in NYC are given in Fig.2. The data at
262 the Central Park site (40.778° N, 73.969° W), a NWS/NOAA weather station, are also given. First, a heat-
263 wave event is indicated on June 11-13 when the maximum temperature is higher than 32.2 ˚C. At noon, the
264 temperature was highest (37.5 ˚C) at IS-52 (located in Bronx) but close for other sites. Secondly, large
265 differences of temperature of ~8 ˚C at the urban and suburb site (IS52 vs. White Plains-WP) at night
266 indicated the significant effect of the urban heat island. The prevailing western and southwest winds with
267 horizontal velocity less than 7 m/s in Fig.2 (b) were observed on June 11-13; this indicates that Long Island
268 and Long Island Sound (LIS) are in the NYC downwind area. The heat-wave event ended with a decrease
269 temperature and some scattered shower in the morning of June 14 (shown by the ceilometer data later).

270 The daily O_3 air quality index (AQI) map on June 12 is given in Fig.3. The regional unhealthy air
271 (color in orange and red) is illustrated in NYC area. The tropospheric column NO_2 product on June 12 from
272 the Ozone Monitoring Instrument (OMI) observations on the NASA AURA satellite, indicate a high or
273 "hot" NO_2 area in NYC (not shown here). The temporal variation of O_3 concentration in NYC area is given
274 in Fig.4. The 8-hr average of O_3 mixing-ratio attains 89 ppb and exceeds the NAAQS (70-ppb) while the
275 ground $PM_{2.5}$ showed an increasing trend from 10 to 25- $\mu g/m^3$ in Fig.6. Importantly, O_3 concentrations in
276 the NYC downwind suburb (e.g. Suffolk, Babylon and Riverhead) are much higher than those in the urban
277 area (e.g. CCNY, NYBG and IS52). For instance, the peak value of O_3 mixing ratio reached 110 ppb at
278 Riverhead and Babylon but 70~80 ppb at CCNY and QC on June 12 and 13, which might be associated
279 with the combined effects of urban pollution transport, favorable local meteorological and chemical process
280 in the coastal environment (Miller, 2017). As shown in Fig.2 (b), during June 10~13, the prevailing western
281 and southwest winds (velocity at 2~7 m/s) in the NYC area result in the transport of urban air pollution to

282 the coastal area. Further analysis with comprehensive observation at the urban-coastal area and high spatial-
283 resolution weather/air quality model are highly needed.

284 The temporal variability of the $PM_{2.5}$ and its compositions (OC, EC and sulfate SO_4^{2-}) is shown in
285 Fig.5. First, the total $PM_{2.5}$ measured at multiple sites indicated a consistent increase trend on the heat-wave
286 days. A consistent enhancement of OC and sulfate can be seen at QC site. For instance, the OC increased
287 from 2 $\mu g/m^3$ on June 9 to 6.8 $\mu g/m^3$ on June 12-13 while the sulfate increased from 0.4 $\mu g/m^3$ on June 8-9
288 to 3.0 $\mu g/m^3$ on June 13. These increments were likely due to the secondary formation of aerosols through
289 the chemical reactions. On the other hand, the EC generally shows high value at the traffic rush hours at
290 6:00 am ~ 7:00 am EDT or local time in the morning, attributed to the primary emissions from the vehicles.
291 There were some scattered rainfall on June 14 and 16 (not shown here) that resulted in wet scavenging of
292 ground $PM_{2.5}$. Figure 6 gives the main speciation of $PM_{2.5}$ from the 1-in-3 day 24-hr integrated-filter
293 observations in the NYC area. A coincident high-level of OM and sulfate occurred on the heat-wave day
294 of June 12 at all three-site; and the OM concentration is dominant in the total $PM_{2.5}$. On June 12, the
295 fractional contribution to the total $PM_{2.5}$ was in range of 51%~58% from the OM and 12%~14% from
296 sulfate at the three sites. The results agree well with the hourly observations in Fig.5.

297 Based on the available data measured at the NYSDEC stations, we compare the spatial difference
298 of sulfate, BC and SO_2 in the urban (QC or IS52-site), suburban (Suffolk) and rural area (WF-Whiteface,
299 and Pinnacle). The results are shown in Fig.7. At first, the sulfate at both QC and Whiteface sites showed
300 significant enhancement on the heat-wave days of June 11-13 in Fig.7a, but the sulfate at QC site (~3 $\mu g/m^3$)
301 was larger than those at the Whiteface site (~2 $\mu g/m^3$) on June 13, attributed to more urban emissions and
302 chemical formation. Before and after the heat-wave day on June 9 and June 15-17, respectively, the sulfate
303 was at the similar level at both sites. Secondly, the SO_2 at the urban site (QC) in Fig.7 (b) was much higher
304 than that at the suburban site (Suffolk) on June 12-13, both were far below the NAAQS for SO_2 (1-hr 75
305 ppb). Thirdly, the BC in Fig.7(c) showed much larger values at the urban site than those at both rural sites,
306 with a maximum of 2.3 $\mu g/m^3$ at the urban-site but ~0.6 $\mu g/m^3$ at the rural sites on June 13. A high
307 correlation (R^2>0.96) between the BCUV370 and BC880 along with a linear slope of 1.01 at the urban site

indicates that the BC sources are mainly from the vehicles (Rattigan et al., 2013). Meanwhile, the NO_2 and NO showed higher values at the traffic rush hours at the QC and IS-52 sites, which corresponds to the major vehicles emissions in the morning. We note that the QC-site is closer to the highway (e.g. Long Island Express way or I-495). The results above indicate the incremental emissions on the heat-wave days and in the urban area.

3.2 Diurnal variation of PBLH

The temporal variation of PBL-height (PBLH) is estimated from the ceilometer, wind lidar, and CCNY-aerosol lidar, respectively. Figure 8 gives the attenuated backscatter, PBLH, residual-layer-height, and cloud-base from a ceilometer observation during June 10-14. The PBLH shows a strong diurnal variation of 0.2 to 2.5 km from the early morning to noon. Significant growth of PBLH from 0.5 km to 2.0 km was observed from 11:00 to 13:00 on June 12 and 13, remaining at high-levels through the afternoon until 20:00, followed with a high residual layer at night. The maximum PBLH was higher on the heat-wave days from June 11 to June 13. Some cumulus clouds were formed on the PBL-top at noon and afternoon of June 12 and 13; and the scattered showers were observed in the early morning of June 14, indicating the end of heat waves.

The vertical wind velocity and its variation measured by the co-located wind Doppler lidar are shown in Fig.9. The convective PBL is indicated by large variance of vertical velocity at 12:00-19:00. The PBLH is then derived and shows a good agreement with the ceilometer results as shown in Fig. 10. In addition, other aloft-layer convection in the early hours of June 13 is observed. There are no data available below 0.4 km altitude limited by our initial configuration of lidar software. Figure 10 shows the PBLH and time-height distribution of aerosols from the CCNY-lidar observation. The PBLH generally agrees with the ceilometer product, in particular for the rapid growth at 11:00-13:00 on June 12. A strong linear correlation (R=0.94) between the CCNY-lidar and ceilometer result is indicated. Again, few cumulus clouds on the top of PBL are observed, which might be triggered by the upward motion. The clouds can shield the lowest layers of the troposphere from UV radiation that drives photochemical smog (Dickerson et al. 1982). Figure

11 gives the corresponding temporal variations of PBLH, ground O_3 and $PM_{2.5}$ at CCNY-site. In the morning and late evening, both the PBLH and O_3 are low while the ground $PM_{2.5}$ are high. On the contrary, at noon and afternoon, the PBLH and O_3 become higher while the ground $PM_{2.5}$ become relatively lower. Generally, higher PBLH indicates larger air volume for the pollutant dilution and thus results in less pollutants at noon on the ground such as the PM2.5, but strong chemical process at noon also produces more O_3 in the PBL and ground level.

To demonstrate how well the ceilometer-measured backscatters represent the ground $PM_{2.5}$ in NYC, we calculate their correlation during this heat-wave event. Figure 12 gives their correlations at the near range. A good correlation at near surface (R=0.89) is indicated, and such high correlation may occur up to 200-m attitude where the correlation coefficient R is around 0.8. This means that the ceilometer-measured near-range backscatter may be a good proxy of ground $PM_{2.5}$ loading on the heat-wave days.

Using the CCNY multiple-wavelength lidar, the aerosol backscatter and Angstrom exponents on June 12 are derived and shown in Fig.13. At the PBL-top, high aerosol backscatters occur which might indicate the hydration of aerosols. In the PBL, the Angstrom exponents increase from morning to the afternoon, which probably indicates fine-mode particle formation. In addition, the total aerosol optical depth (AOD) and Angstrom exponent (AE) measured by the CIMEL-sunphotometer indicatea coincident increase that is suggestive of increase in fine-mode aerosols; and this is consistent with the increase in OC and sulfate aerosols shown earlier as well as the CCNY-lidar retrievals.

The radiosonde-measured profiles of the meteorological parameters are analyzed on June 12-13 in NYC area (OKX site). The results are given in Fig.14. The temperature and potential temperature profiles clearly indicate the PBLH at around 2.0-2.3 km on June 12, which is consistent with the ceilometer and lidar results. Secondly, the temperature inversion occurs at near surface at 8:00 pm EDT. By comparing the vertical profiles of H_2O mixing ratio to the ceilometer-attenuated backscatter, we can see their similar shape of vertical distribution in the PBL. Both show a sharp decrease at the PBL-top.

Finally, in order to observe regional spatial distribution of aerosols and PBLH, the NASA spaceborne lidars (CALIOP and CATS) data in NYC area are shown in Fig.15. The CALIPSO overpass

time was 7:18 UTC (3:18 EDT) on June 12 while the CATS overpass time was 1:00 UTC on June 12 (21:00 on June 11 EDT). The attenuated backscatter profiles along the latitude are plotted for the CALIPSO at 532-nm and CATS 1064-nm, depending on the good SNR, respectively. The high aerosol layers in the northeast US can be seen on both the images. The maximum gradient variation of aerosol backscatter profiles along the track are calculated, which represent the height of nocturnal residual layer. The results are consistent with the ceilometer observations in NYC. Even in the coastal NYC and adjacent Atlantic Ocean, the CATS data still show high aerosol residual layer according to the Level-2 aerosol extinction coefficients (not shown here).

3.3 Comparison to the NAQFC numerical products

With the profiling and ground in-situ data, the NAM-CMAQ numerical products of temperature, PBLH, O_3 and $PM_{2.5}$ are evaluated in NYC area. Firstly, we compare the results at CCNY site in Fig.16. Both the model and observation results show consistent diurnal variation trend for the temperature, PBLH and O_3 except for $PM_{2.5}$. Under the convective PBL conditions at noon and afternoon, the model products (temperature, O_3 and $PM_{2.5}$) show good agreement with near surface observations on June 12 - 13. However, in the morning and at night, the model products indicate an underestimate of temperature, PBLH and O_3, but a dramatic overestimate of $PM_{2.5}$ in comparison to the observations. To explore the vertical distribution of O_3 and $PM_{2.5}$, we further plot the model data in the lowest 5-layer near the ground (i.e. 0, 40, 80, 120 and 160 m altitude). The O_3 concentrations increase with the altitude whereas the $PM_{2.5}$ decrease with the altitude in the early morning and night, but they vary little at noon and afternoon. Their variations with the altitudes are likely related to weak vertical mixing and their emissions or formation differences.

We made another comparison at QC-site where the NO_2 and NO are measured (not shown here). For the NO_2 and NO, the model products show an overestimate in the morning and night, but good agreement at noon and afternoon. Again, the ground temperature is under-predicted by 3~5˚C in the morning and night. The bias behaviors of modeling O_3 and $PM_{2.5}$ from the observation are similar with the comparisons in Fig.16. Overall, the model shows good performance for the PBLH, $PM_{2.5}$ and O_3 at noon

and afternoon when the PBL is strongly convective. The large biases are seen in the early morning and night, which are probably associated with weak mixing process and lower PBLH.

3.4 Discussions

From the ceilometer and lidar observations, we can see good consistency between the aerosol gradient-based and turbulence-based convective PBLH; in the late afternoon after 19:00 EDT, their discrepancy becomes large because of weaker vertical convection and residual aerosol layers. Unfortunately, the wind lidar collected the data with the lowest range at 400-m, thus, lower turbulence-based PBLH at night and early morning could not be obtained. In addition, both the ceilometer and CCNY-lidar observed the formation of cumulus clouds on the PBL-top at noon and afternoon. The clouds can shield the lowest layers of the troposphere from UV radiation that drives photochemical smog for the secondary formation of O_3 and aerosols (Dickerson et al. 1982), which may partially result in the spatial difference of O_3 production in NYC area. Cumulus clouds also vent the PBL, moving pollutants into the free troposphere where residence times are longer and impacts are larger (Loughner et al. 2011). Moreover, sulfuric acid is produced rapidly by reaction between sulfur dioxide (SO_2) and hydrogen peroxide (H_2O_2) in cloud droplets; this pathway is the major source of sulfate that contribute to total $PM_{2.5}$ (Zhang et al., 2011). In addition, a deep PBL is observed during the heat-wave periods on June 11-13, which means that air pollutants might be mixed into a greater volume, and the ground-level concentrations are reduced by dilution. This occurs for the ground $PM_{2.5}$ but not for the O_3 as shown by this study, probably due to dominant chemical formation for the O_3 at noon and afternoon.

A consistent increase of OC and sulfate of aerosols are clearly observed during the heat-wave days, even at noon and with a growing PBLH, which indicates strong chemical formation of secondary aerosols. We analyzed the ratio of OC-to-EC during the heat-wave periods. At QC-site, the hourly OC/EC ratios are significantly higher (peak value at 13~15 at noon) on June 11-13 than those (peak value at 6.5~9) on other days (none heatwave days). They are also larger than the previous monthly average values given by Rattigan (2010). The OC/EC ratios show a minimum at ~4 at nights of June 12 and 13, but at ~1.7 at night of June

9 before the heatwave. Overall, the large OC/EC ratios on heatwave days clearly indicate strong formation of secondary organic aerosols (SOA); and they can largely contribute to the total $PM_{2.5}$. In addition, the ratios of OC-to-sulfate become slightly lower on the heatwave days of June 12-13.

In addition, the O_3 in the downwind area of NYC (e.g. Riverhead, Babylon and Suffolk in Long Island) showed much higher concentrations (~110 ppb) than those (~70-80 ppb) in the urban sites (e.g. CCNY and QC) for this heat-wave event when the prevailing winds are westerly in NYC. The higher O_3 in the Long Island is probably associated with the urban pollution transport and local meteorological conditions (Goldberg et al., 2014, Miller, 2017; Zhao et al., 2019). Comprehensive surface and range-resolved observations of O_3, its precursors and meteorological parameters are needed to understand the mechanisms of high-level ground O_3 in the urban and coastal environment (Miller, 2017).

Under the convective PBL period (12:00-19:00 EDT), the NAM-CMAQ model shows good agreement with the observations for the near-surface O_3, $PM_{2.5}$, NOx, temperature, as well as PBLH. However, in the early morning and night, the model underestimates observed PBLH, and near-surface temperature and O_3, but an overestimates $PM_{2.5}$and NOx. The model predicted temperatures are colder by 3~5 ˚C and PBLH lower compared to the observations in NYC, indicating weaker vertical mixing (Gerbig et al, 2008). As demonstrated by Gutiérrez et al. (2015) and Ortiz et al (2018), the urban heat-related BEM and BEP can affect the thermal structure, wind and enhance the vertical mixing in the urban boundary layer. Zhang (2011) indicate that without the upstream urbanization along the Washington–Baltimore Corridor, the UHI effects over Baltimore would be reduced by 25% with a shallower mixed PBL. Zhang (1999) demonstrated that the vertical mixing process contributed significantly to the ozone buildup at ground level in the morning in NYC due to aloft high-O_3.Therefore, an urban-WRF coupled or driven air quality model is highly expected to improve air quality forecast in NYC area. Importantly, the range-resolved profiling observations of O_3, aerosols and meteorological parameters are critical to evaluate the model performance.

4. Conclusion

433 This paper presents a synergistic assessment of heat-wave impacts on the urban air quality and PBLH in
434 June 2017 in New York City. We demonstrate a strong urban-heat-island signal with the temperature
435 difference of ~8 ˚C at night in NYC area. Strong diurnal variation of PBLH is observed from the co-located
436 a ceilometer, wind and aerosol lidars, showing a consistent and dramatic growth of PBLH at 11:00-13:00
437 and followed by a high and stable PBLH at 2.0-2.5 km at noon and afternoon. The regional-scale high
438 residual-layers of aerosols are observed in the NYC vicinity from the space-borne lidars.

439 During the heat-wave periods, the ground O_3 mixing ratios exceed the NAAQS with a maximum
440 of 110 ppb in the areas downwind of NYC whereas the ground $PM_{2.5}$ concentrations are enhanced from 5
441 $\mu g/m^3$ to 25 $\mu g/m^3$. A coincident increase of the OC and sulfate aerosols indicates strong secondary
442 formation of aerosols, with a dominant contribution of OM (52~58%) to the total $PM_{2.5}$. The combined
443 effects of urban pollutant transport and local meteorology may be responsible for the high level of O_3 in the
444 downwind suburb area. Different diurnal variations of ground O_3 and $PM_{2.5}$ are observed, which may be
445 associated with the effects of PBLH evolution and their different formation and emissions processes.

446 The comparisons between the NOAA-NAQFC model products (T, PBLH, O_3, $PM_{2.5}$ and NOx) and
447 the observations clearly show good consistency under the convective PBL periods at noon and afternoon.
448 Yet, in the early morning and night, the model products show an underestimate for temperature, PBLH and
449 O_3, but an overestimate of $PM_{2.5}$ and NOx. Such discrepancies are probably associated with the weak
450 vertical mixing or PBL-height underestimate and anthropogenic emissions in the model.

451 **Acknowledgements.** This study is partly supported by the New York State Energy Resources Development
452 Authority (NYSERDA grant # 100415 and 137482), and The National Oceanic and Atmospheric
453 Administration – Cooperative Science Center for Earth System Sciences and Remote Sensing
454 Technologies (NOAA-CREST) under the Cooperative Agreement Grant # NA16SEC4810008. Authors
455 greatly appreciate the data from NOAA, NYSDEC, NASA-AERONET, CALIPSO and CATS. In particular,
456 we appreciate Oliver Rattigan for providing OC/EC data and reviewing this paper. Although the manuscript
457 was reviewed internally, it does not necessarily reflect the views or policies of the New York State
458 Department of Environmental Conservation. We gratefully acknowledged the constructive comments from
459 two anonymous reviewers that improve the manuscript.
460

References

Bae, M.S., Demerjian, K.L. and Schwab, J.J., 2006. Seasonal estimation of the organic mass to organic carbon in PM2.5 at rural and urban locations in New York state. *Atmos. Environ.* 40: 7467–7479.

Bauer, J. J., X.Y. Yu, R. Cary, N. Laulainen, C. Berkowitz, 2009. Characterization of the Sunset Semi-Continuous Carbon Aerosol Analyzer, J. Air & Waste Management Assoc. 59:7, 826-833.

Brooks, I., 2003. Finding boundary layer top: Application of a wavelet covariance transform to lidar backscatter profiles, J. Atmos. Oceanic Technol., 20, 1092-1105.

Castellanos, P., L. T. Marufu, B. G. Doddridge, B. F. Taubman, J. J. Schwab, J. C. Hains, S. H. Ehrman, R. R. Dickerson, 2011. Ozone, oxides of nitrogen, and carbon monoxide during pollution events over the eastern United States: An evaluation of emissions and vertical mixing. J. Geophy. Res., **116**:D16.

Cohn, S. A., Angevine, W. M., 2000. Boundary layer height and entrainment zone thickness measured by lidars and wind-profiling radars, J. Appl. Meteorol., 39, 1233– 1247.

Dickerson, R. R., Stedman, D. H., Delany, A. C., 1982. Direct measurements of ozone and nitrogen dioxide photolysis rates in the troposphere, J. Geophys. Res., 87(C7), 4933– 4946.

Draxler, R.R., Hess, G.D., 1997. Description of the HYSPLIT_4 modeling system. NOAA Tech. Memo. ERL ARL-224, NOAA Air Resources Laboratory, Silver Spring, MD, 24.

Gan, C., Wu, Y., Madhavan, B., Gross, B., Moshary, F., 2011. Application of active optical sensors to probe the vertical structure of the urban boundary layer and assess anomalies in air quality model PM2.5 forecasts, *Atmos. Environ.*, 45 (37), 6613-6621.

Gerbig, C., Körner, S., Lin, J. C., 2008. Vertical mixing in atmospheric tracer transport models: error characterization and propagation, Atmos. Chem. Phys., 8, 591-602.

Goldberg, D. L., C. P. Loughner, M. Tzortziou, J. W. Stehr, K. E. Pickering, L. T. Marufu, R. R. Dickerson, 2014. Higher surface ozone concentrations over the Chesapeake Bay than over the adjactent land: Observations and models from the DISCOVER-AQ and CBODAQ campaigns, *Atmos. Environ,* **84**, 9-19.

Gutiérrez, E., J.E. González, A. Martilli, R. Bornstein, M. Arend, 2015. Simulations of a Heat-Wave Event in New York City Using a Multilayer Urban Parameterization. J. Appl. Meteor. Clima, **54**, 283–301.

Haeffelin, M., Angelini, F., Morille, Y., Martucci, G., Frey, S., Gobbi, G.P., Lolli, S., O'Dowd, C. D., Sauvage, L., Xueref-Rémy. I., Wastine, B., Feist, D. G., 2012. Evaluation of mixing-height retrievals from automated profiling lidars and ceilometers in view of future integrated networks in Europe, Boundary Layer Meteorol., 143, 49– 75

Haman, C. L., E. Couzo, J. H. Flynn, W. Vizuete, B. Heffron, B. L. Lefer, 2014. Relationship between boundary layer heights and growth rates with ground-level ozone in Houston, Texas, *J. Geophys. Res. Atmos.*, 119, 6230–6245.

Hogrefe, C., W. Hao, K. Civerolo, J. Ku, G. Sistla, R. Gaza, L. Sedefian, K. Schere, A. Gilliland, R. Mathur, 2007. Daily Simulation of Ozone and Fine Particulates over New York State: Findings and Challenges. J. Appl. Meteor. Clim., 46, 961–979.

Holben, B.N., T. F. Eck, I. Slutsker, D. Tanré, J.P. Buis, A. Setzer, E. Vermote, J.A. Reagan, Y.J. Kaufman, T. Nakajima, F. Lavenu, I. Jankowiak, A. Smirnov, 1998. AERONET - A federated instrument network and data archive for aerosol characterization, Rem. Sens. Environ., 66, 1-16.

Horton, R. M., J. S. Mankin, C. Lesk, E. Coffel, C. Raymond, 2016. A Review of Recent Advances in Research on Extreme Heat Events. *Current Climate Change Reports* 2:4, 242-259.

Hou, P. and Wu, S., 2016. Long-term Changes in Extreme Air Pollution Meteorology and the Implications for Air Quality. *Sci. Rep.* 6, 23792.

Hu, X. M., P. M. Klein, M. Xue, F. Zhang, D. C. Doughty, R. Forkel, E. Joseph, J. D. Fuentes, 2013. Impact of the vertical mixing induced by low-level jets on boundary layer ozone concentration. Atmos. Environ., **70**, 123-130.

Huang, J., J. McQueen, J. Wilczak, I. Djalalova, I. Stajner, P. Shafran, D. Allured, P. Lee, L. Pan, D. Tong, H. Huang, G. DiMego, S. Upadhayay, L. Monache, 2017. Improving NOAA NAQFC $PM_{2.5}$ predictions with a bias correction approach, Wea. and Forecasting, 32, 407-421.

Klein, P. M., X.-M. Hu, M. Xue, 2014. Impacts of Mixing Processes in Nocturnal Atmospheric Boundary Layer on Urban Ozone Concentrations. Bound.-Layer Meteor. 150, 107–130.

Lau, N. and M. J. Nath, 2012. A Model Study of Heat Waves over North America: Meteorological Aspects and Projections for the Twenty-First Century. *J. Climate,* 25, 4761–4784.

Lee, P., J. McQueen, I. Stajner, J. Huang, L. Pan, D. Tong, H. Kim, Y. Tang, Kondragunta S., M. Ruminski, S. Lu, E. Rogers, R. Saylor, P. Shafran, H. Huang, J. Gorline, S. Upadhayay, R. Artz, 2016. NAQFC developmental forecast guidance for fine particulate matter (PM2.5). Wea. and Forecasting. doi:10.1175/WAF-D-15-0163.1.

Li, D, Bou-Zeid, E., 2013. Synergistic interactions between urban heat Islands and heat waves: the impact in cities is larger than the sum of its parts J. Appl. Meteorol. Climatol. 52, 2051–64

Loughner, C. P., Allen, D. J., Pickering, K. E., Dickerson, R. R., Zhang, D.L., Shou, Y. X., 2011. Impact of fair-weather cumulus clouds and the Chesapeake Bay breeze on pollutant transport and transformation. *Atmos. Environ.*, **45**, 4060–4072.

Meehl, G. A, 2004. More Intense, More Frequent, and Longer Lasting Heat Waves in the 21st Century. Science. 305 (5686): 994–7.

Menut, L., Flamant,C., Pelon,J., Flamant, P. H., 1999. Urban boundary-layer height determination from lidar measurements over the Paris area, Appl. Opt. **38**, 945-954.

Miller, P. J., 2017. Retrospective and Future Analysis of Air Quality In and Downwind of New York City, DRAFT White Paper, available at www.nescaum.org/documents/listos.

New York State Energy Research and Development authority, Assessment of carbonaceous PM2.5 for New York and the region, final report 08-01, Vol. ii, March 2008.

Ortiz, L.E., J.E. Gonzalez, W. Wu, M. Schoonen, J. Tongue, and R. Bornstein, 2018. New York City Impacts on a Regional Heat Wave. *J. Appl. Meteor. Climatol.,* **57**, 837–851.

Ramamurthy, P., J. González, L. Ortiz, M. Arend, F. Moshary, 2017. Impact of heatwave on a megacity: an observational analysis of New York City during July 2016, Environ. Res. Lett., 12(5), 054011

Rattigan, O. V., H. D. Felton, M.S. Bae, J. J. Schwab, K. L. Demerjian, 2010. Multi-year hourly PM2.5 carbon measurements in New York: Diurnal, day of week and seasonal patterns, Atmos. Environ., 44 (16), 2043-2053.

Rattigan, O. V. , K. Civerolo, P. Doraiswamy, H. D. Felton, P. K. Hopke, 2013. Long Term Black Carbon Measurements at Two Urban Locations in New York, Aerosol and Air Quality Res., 13: 1181–1196.

Rattigan, O. V., K. L. Civerolo, H. D. Felton, J. J. Schwab, K. L. Demerjian, 2016. Long Term Trends in New York: $PM_{2.5}$ Mass and Particle Components, Aerosol and Air Quality Res., 16(5), 1191-1205.

Robinson, P. J., 2001. On the Definition of a Heat Wave. Journal of Applied Meteorology. 40 (4): 762–775

Schnell, J. L., Prather, M. J., 2017. Co-occurrence of extremes in surface ozone, particulate matter, and temperature over eastern North America. *Proc. National Academy of Sciences of the United States of America*, *114*(11), 2854–2859.

Schween, J. H., A. Hirsikko, U. Löhnert, S. Crewell, 2014. Mixing-layer height retrieval with ceilometer and Doppler lidar from case studies to long-term assessment, Atmos. Meas. Tech., 7, 3685–3704.

Shen, L., L. J. Mickley, E. Gilleland, 2016. Impact of increasing heatwaves on U.S. ozone episodes in the 2050s: Results from a multi-model analysis using extreme value theory**.** *Geophysical Research Letters*, DOI: 10.1002/2016GL068432.

Tressol, M., C. Ordonez, R. Zbinden, Jérôme Brioude, V. Thouret, 2008. Air pollution during the 2003 European heat wave as seen by MOZAIC airliners. Atmos. Chem. and Phys. 8(8), 2150.

Tucker, S. C., C. J. Senff, A. M. Weickmann, W. A. Brewer, R. M. Banta, S. P. Berg, D. C. Law, R. M. Hardesty, 2009. Doppler idar estimation of mixing height using turbulence, shear, and aerosol profiles, J. Atmos. Ocean. Tech. 26, 673-688.

Vaughan, M.A., Powell, K.A., Winker, D.M., Hostetler, C.A., Kuehn, R.E., Hunt, W.H., Getzewich, B.J., Young, S.A., Liu, Z., McGill, M.J., 2009. Fully automated detection of cloud and aerosol layers in the CALIPSO lidar measurements. J Atmos Ocean Technol 26:2034 –2050.

Wiegner, M., S. Emeis, V. Freudenthaler, B. Heese, W. Junkermann, C. Munkel, K. Schafer, M. Seefeldner, S. Vogt, 2006. Mixing layer height over Munich, Germany: Variability and comparisons of different methodologies, J. Geophys. Res., 111, D13201, doi:10.1029/2005JD006593.

Wu, Y., S. Chaw, B. Gross, F. Moshary, and S. Ahmed, 2009. Low and optically thin cloud measurements using a Raman-Mie lidar, Appl. Opt. 48, 1218-1227.

Wu, Y., A. Arapi, J. Huang, B. Gross, F. Moshary, 2018. Intra-continental wildfire smoke transport and impact on local air quality observed by ground-based and satellite remote sensing in New York City, *Atmos. Environ.*, 187, 266-281.

Yegorova, E. A., D. J. Allen, C. P. Loughner, K. E. Pickering, R. R. Dickerson, 2011. Characterization of an eastern U.S. severe air pollution episode using WRF/Chem, *J. Geophys. Res.*, 116, D17306, doi: 10.1029/2010JD015054.

Yorks, J. E., McGill, M. J., Palm, S. P., Hlavka, D. L., Selmer, P. A., Nowottnick, E. P., Vaughan, M. A., Rodier, S. D., and Hart, W. D., 2016. An overview of the CATS level 1 processing algorithms and data products. Geophys Res. Lett., 43,4632–4639.

Zhang, D., Y. Shou, R.R. Dickerson, F. Chen, 2011: Impact of Upstream Urbanization on the Urban Heat Island Effects along the Washington–Baltimore Corridor. *J. Appl. Meteor. Climatol.,* **50**, 2012–2029.

Zhang, J., Rao, S.T., 1999. The role of vertical mixing in the temporal evolution of ground-level ozone concentrations. J. Appl. Meteor., 38, 1674–1691.

Zhao, K., Y. Bao, J. Huang, Y. Wu, F. Moshary, M. Arend, Y. Wang, X. Lee, 2019. A high-resolution modeling study of a heat wave-driven ozone exceedance event in New York City and surrounding regions, Atmos. Environ., 199, 368-379.

582 Zhao, L., M. Oppenheimer, Q. Zhu, J. W Baldwin, E. Bou-Zeid, K. Guan, X. Liu, 2018. Interactions
583 between urban heat islands and heat waves, Environ. Res. Lett. 1(3), 034003.
584

Fig. 1. Ground observation sites in NYC used in this study. (FKW: Fresh Kills West; QC: Queens College; WP: White Plains)

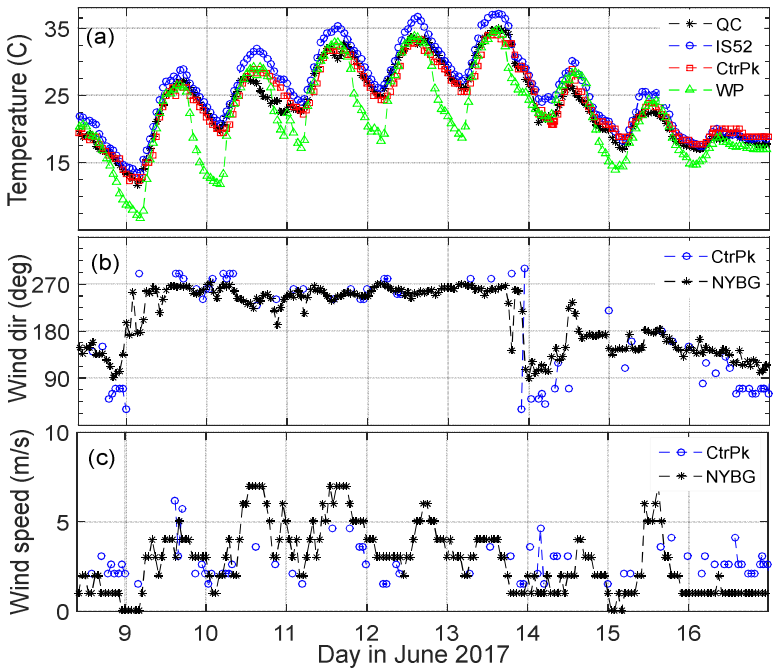

Fig. 2. (a) Air temperature, (b) wind direction and (c) speed measured at the ground sites during June 8-16, 2017. QC-Queens College, WP-White Plains, CtrPk-Central Park, NYBG-NY Botanical Garden.

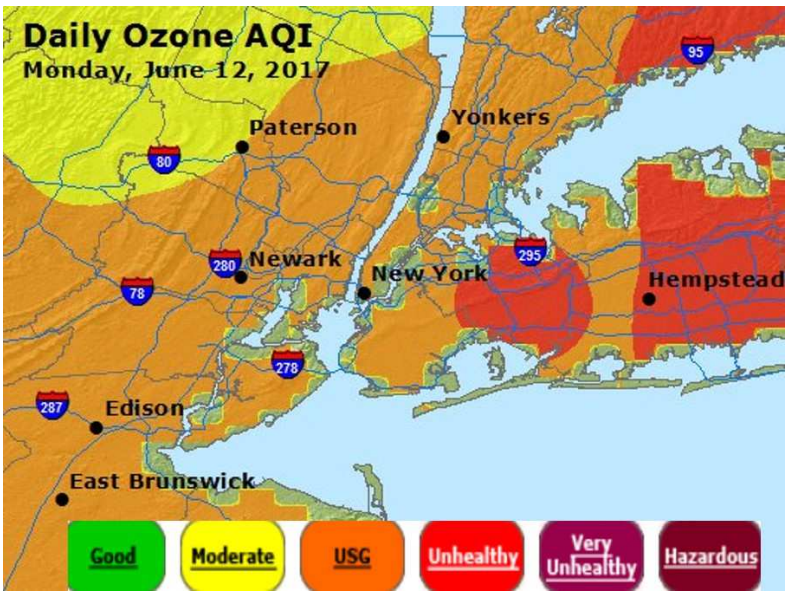

Fig.3. Ozone- air quality index (AQI) in NYC and surrounding area on June 12, 2017. (https://www.airnow.gov)

.

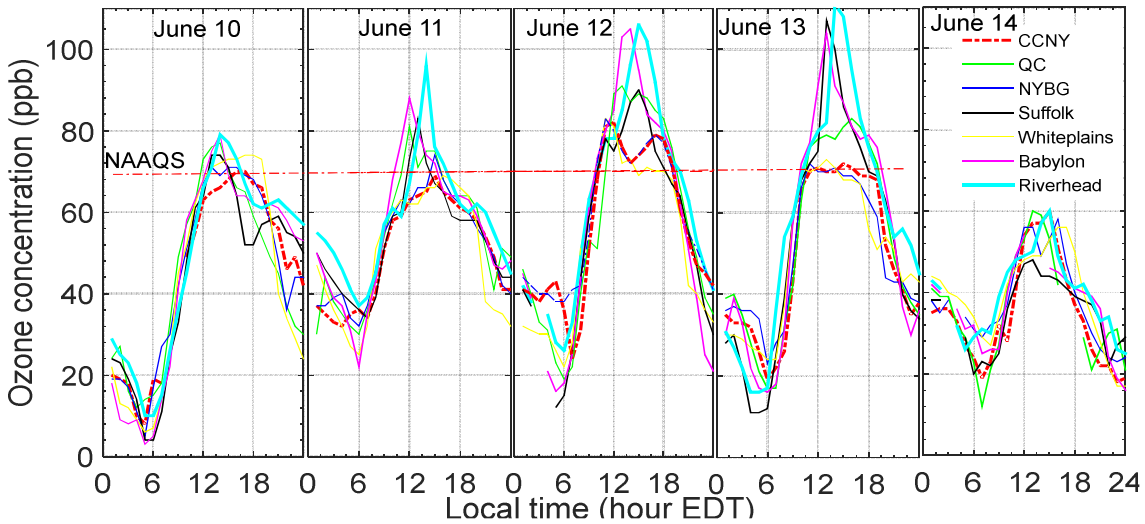

604

605 Fig.4. Hourly O_3 concentration at the ground stations in NYC area during June 10-14, 2017.

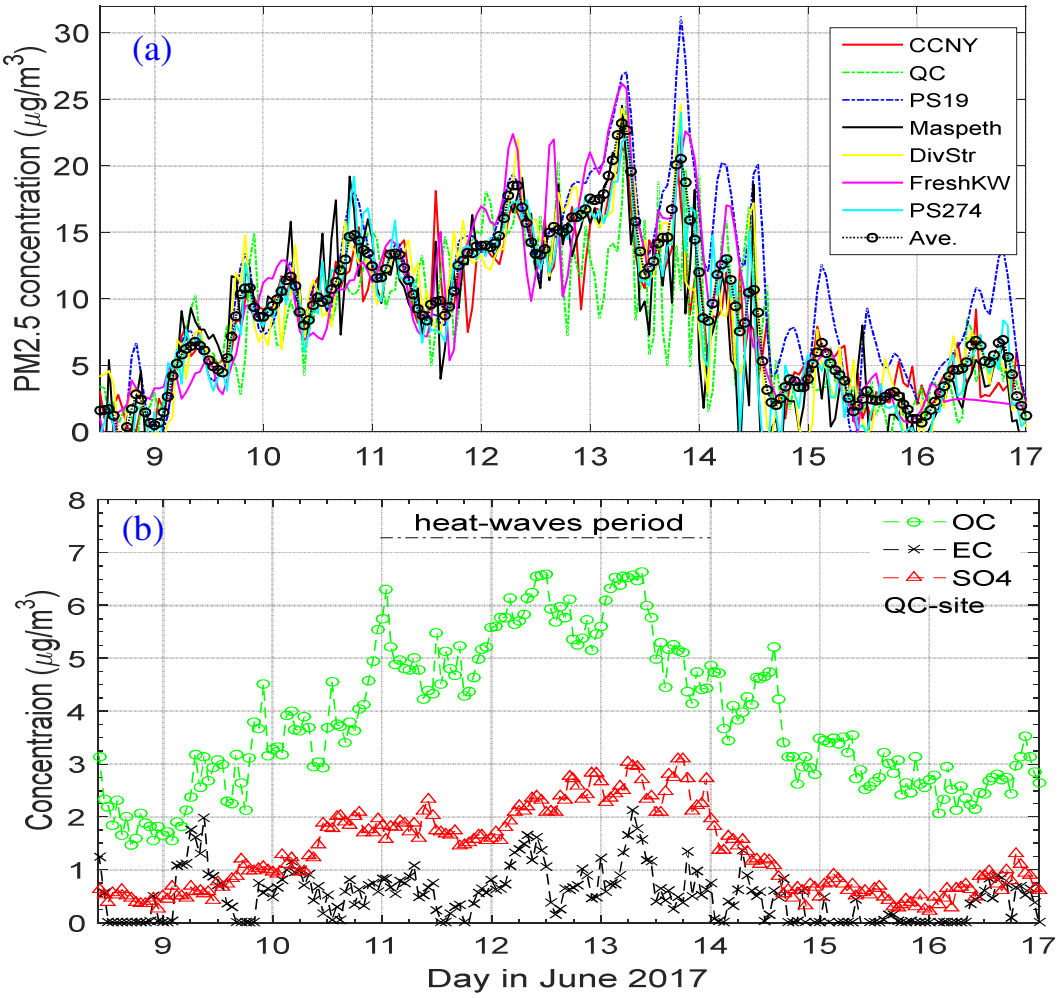

606

607

608 Fig.5 (a)-(b) Hourly $PM_{2.5}$, OC, EC and sulfate at QC and IS-52 sites during June 8-16, 2017.

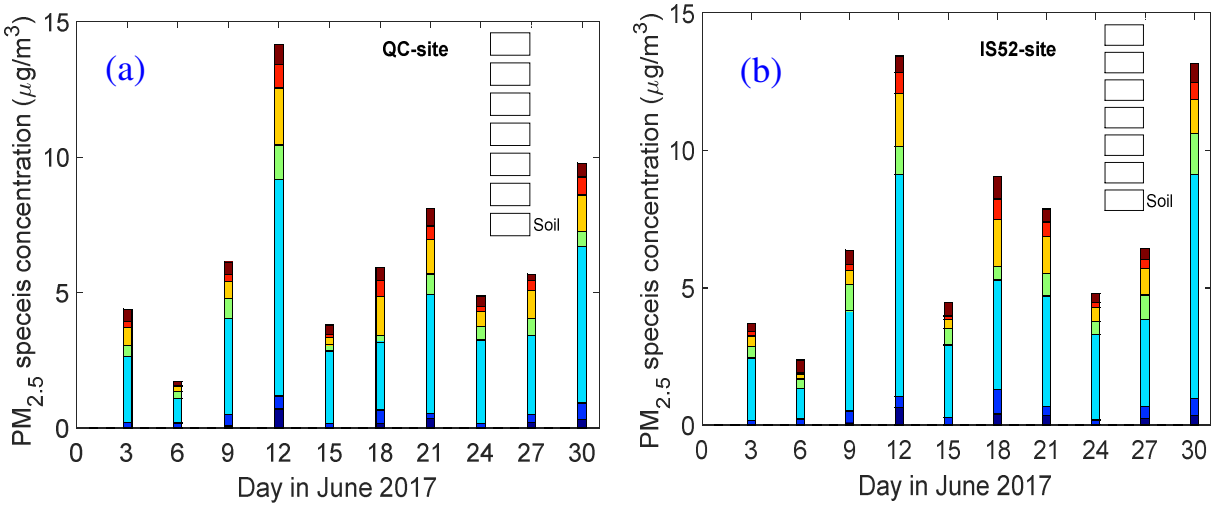

609

610 Fig.6. (a)-(b) Daily (24-h) integrated-filter measured $PM_{2.5}$ species at QC and IS-52 in June 2017

611

612

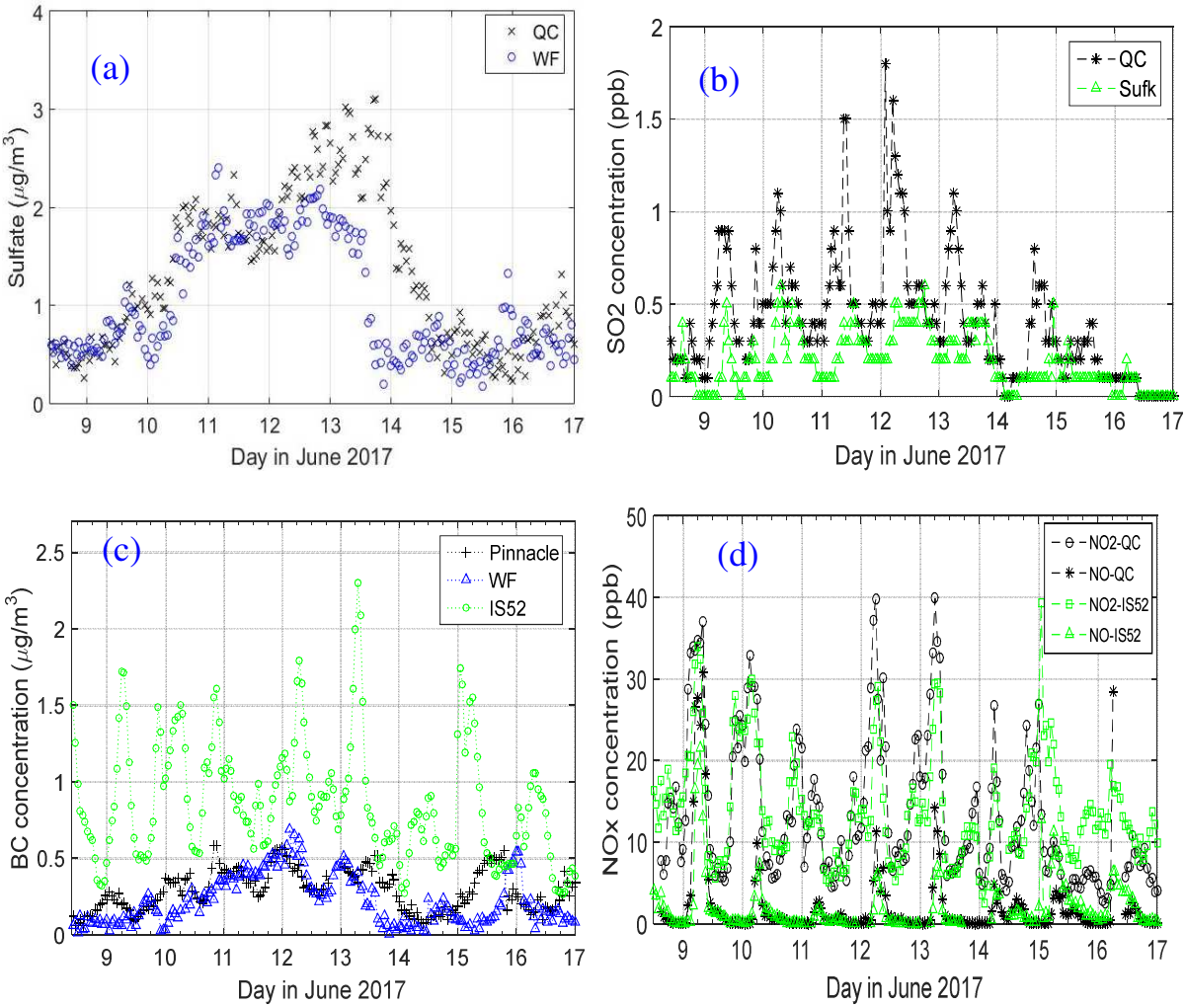

613

614 Fig.7. (a) Sulfate, (b) SO_2, (c) BC and (d) NO_2 and NO measured at the ground stations in NYC

615 surrounding area. (QC-Queens College, WF-Whiteface Mountain, Sufk-Suffolk)

616

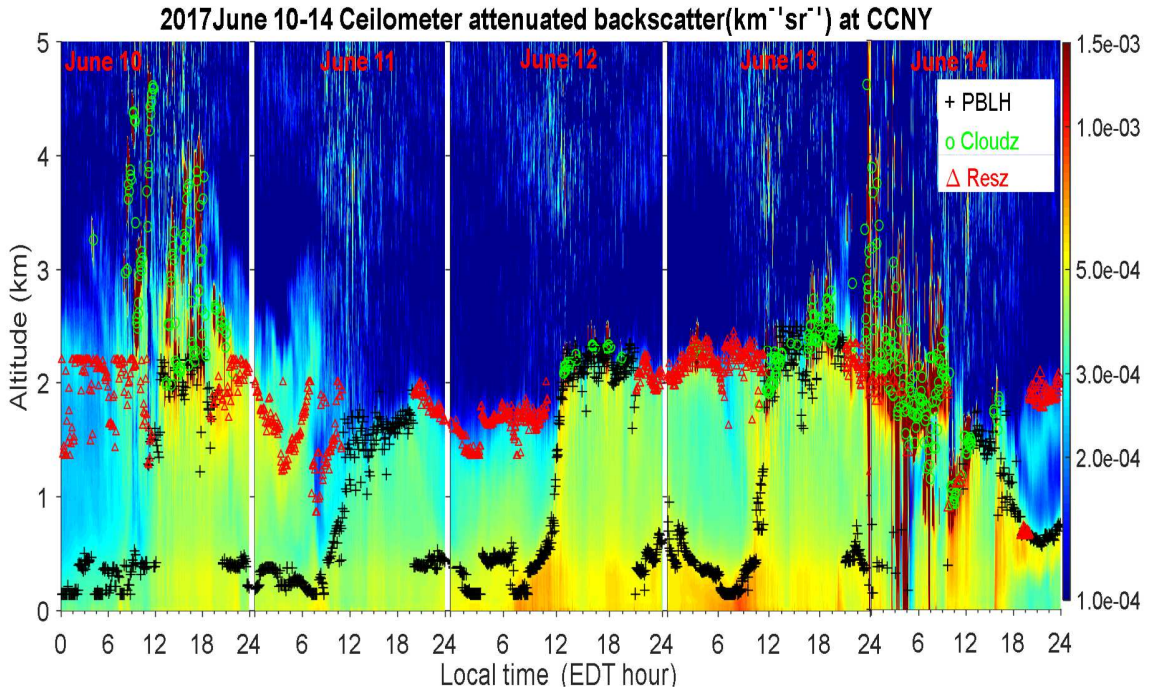

Fig. 8. PBL-height (symbol '+'), residual-layer ('Δ') and cloud-base ('o') observed from the Ceilometer at CCNY during June 10-14, 2017.

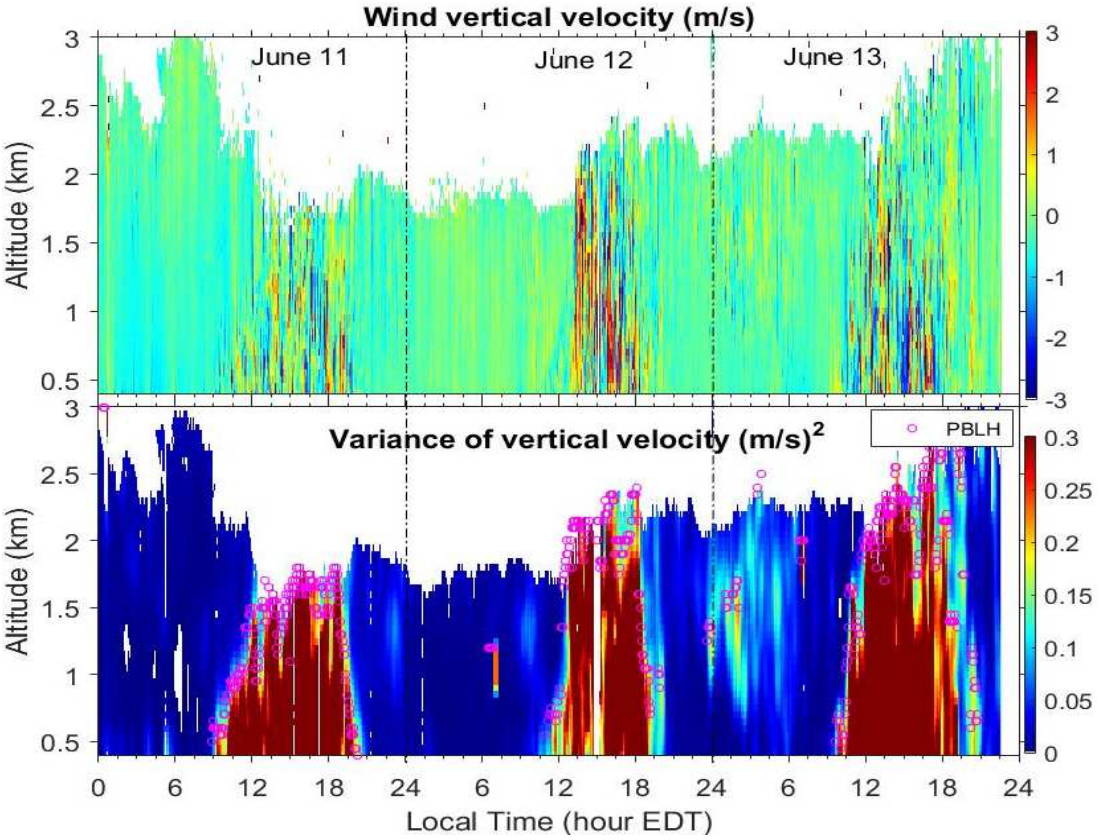

Fig.9. Vertical wind velocity and variance observed by the coherent Doppler wind lidar at CCNY

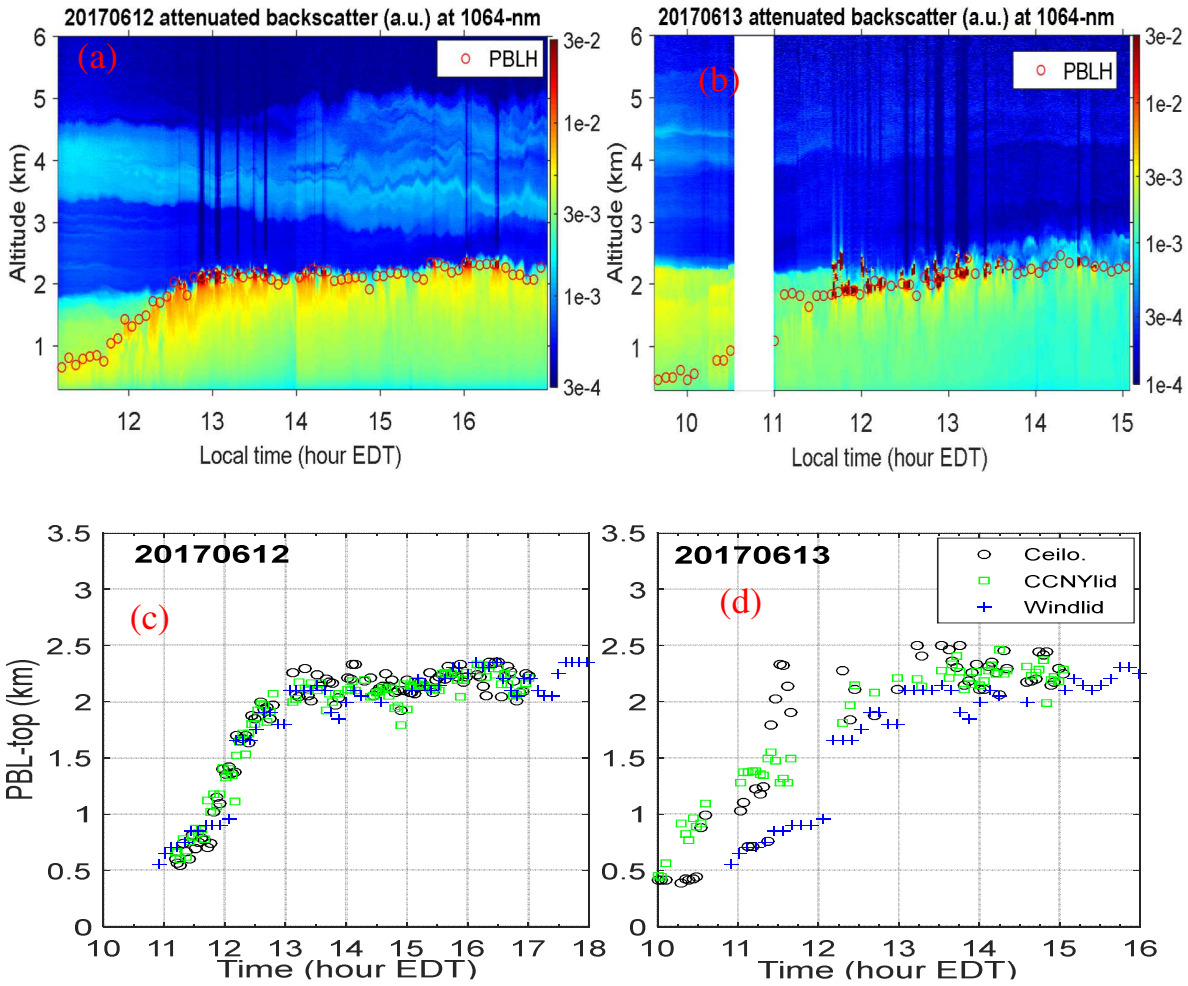

Fig.10. (a)-(b) PBLH (symbol 'o') and aerosol attenuated backscatter from the CCNY-lidar, (c)-(d) PBLH comparison among the ceilometer and lidars on June 12 and 13, 2017. (Ceilo.: ceilometer)

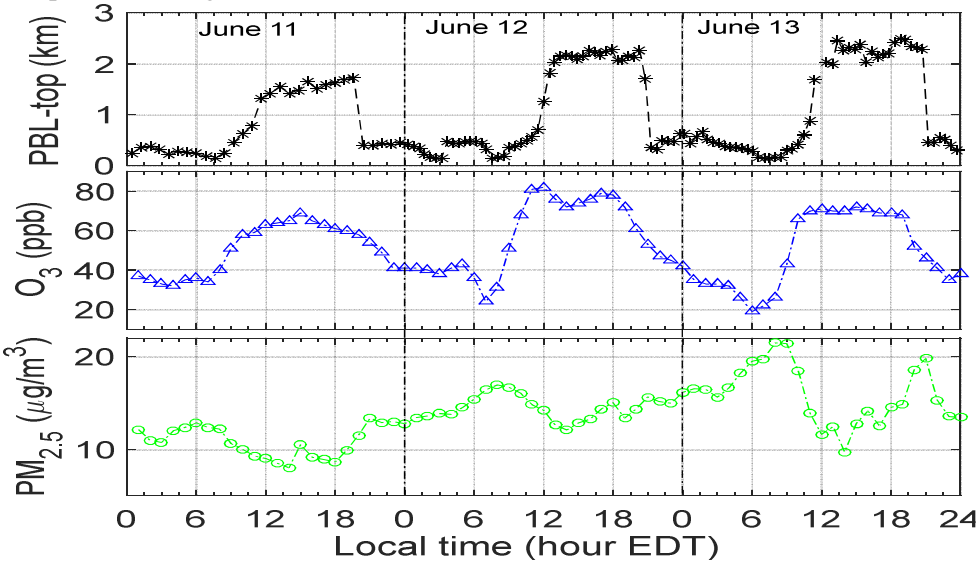

Fig.11. Co-located measurement of PBLH, ground O_3 and $PM_{2.5}$ at CCNY site on June 11-13, 2017

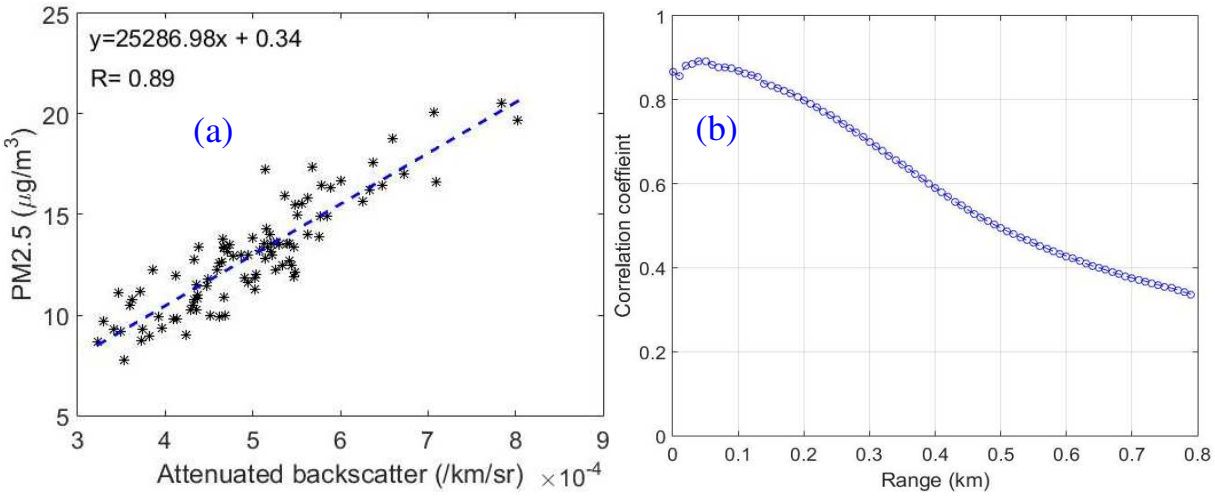

Fig.12 Correlation coefficient between ground $PM_{2.5}$ and ceilometer-attenuated backscatter coefficients during June 10-13 at CCNY. (a) at range of 50-m, (b) at different ranges.

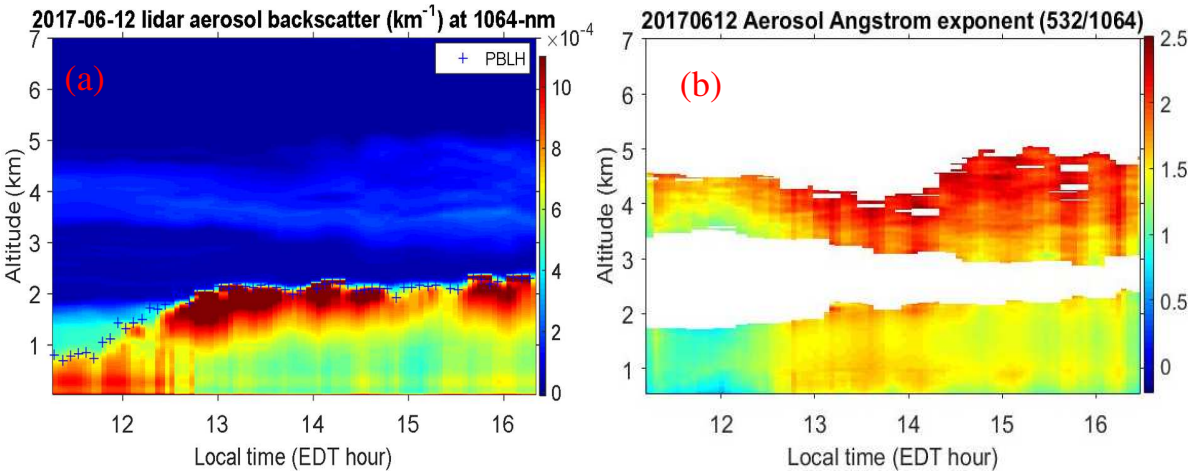

Fig.13. (a) CCNY-lidar derived aerosol backscatter and (b) Angstrom exponent on June 12, 2017.

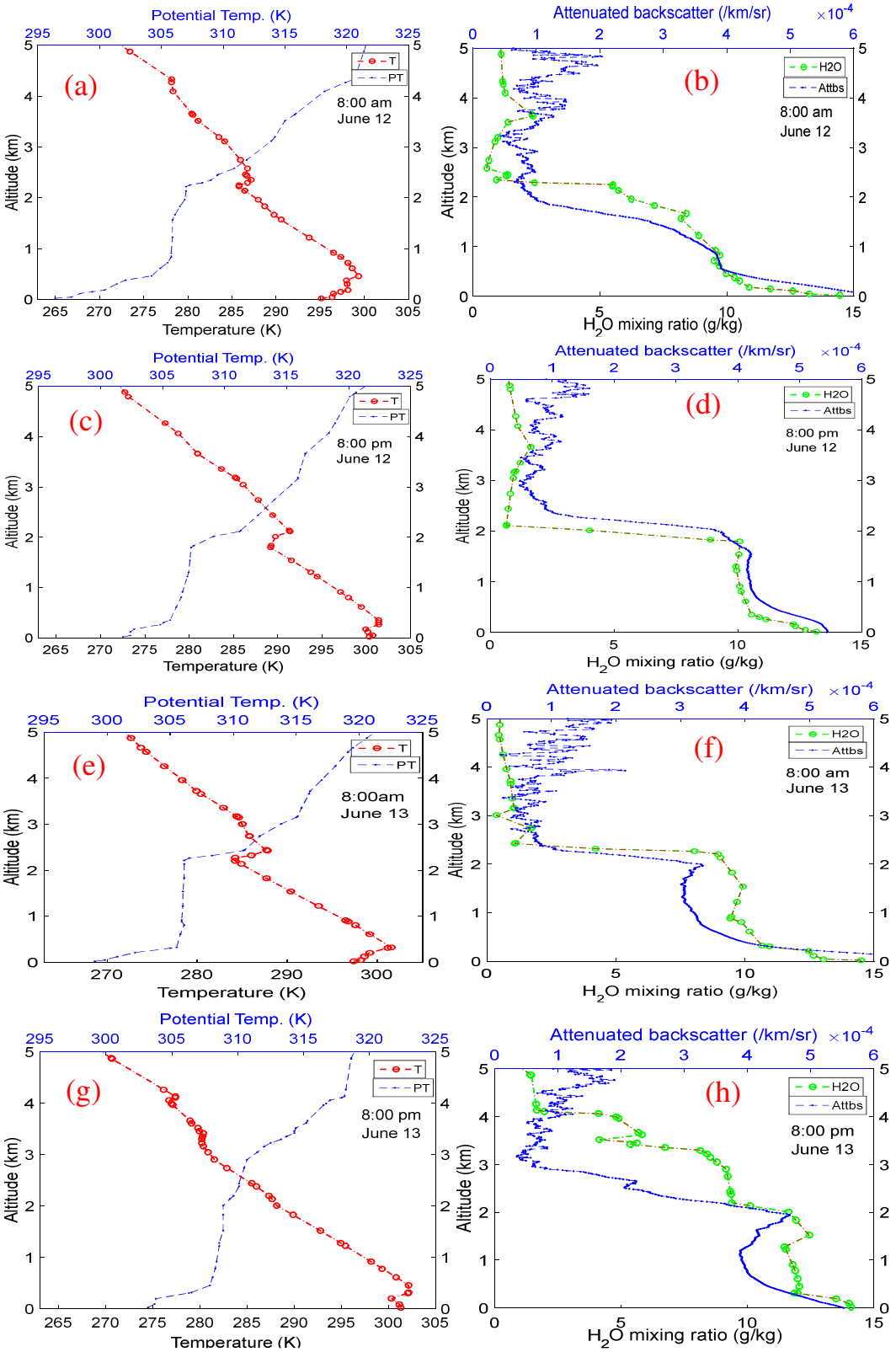

Fig.14. Radiosonde-measured profiles of temperature, potential temperature, water vapor, and ceilometer-measured attenuated backscatter at 8:00 am and 8:00 pm EDT in NYC area on June 12-13, 2017.

643

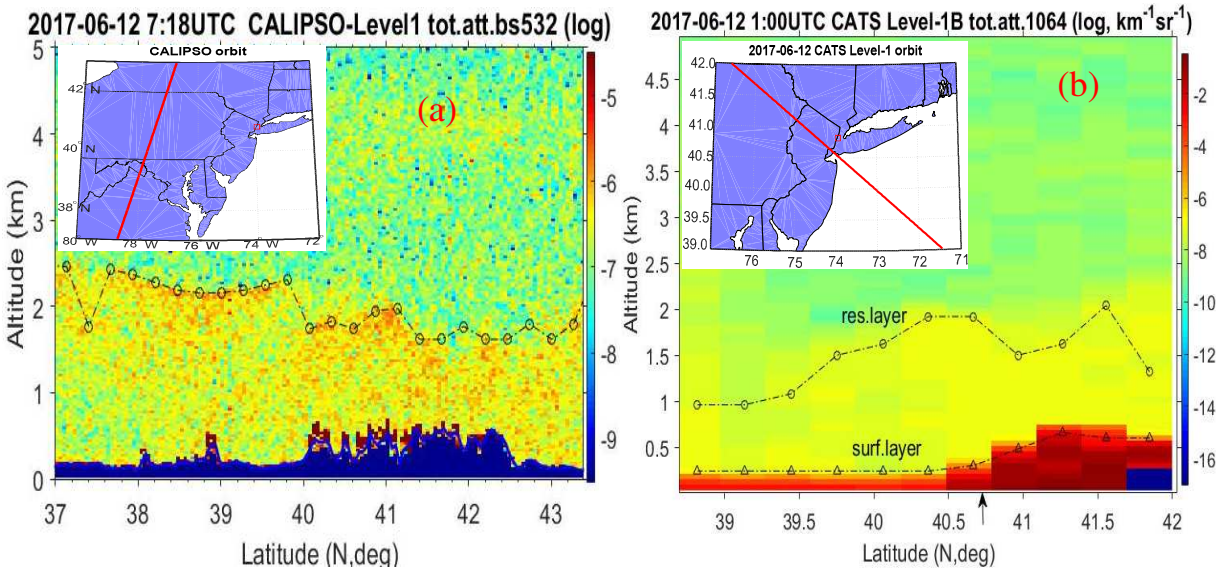

644

645 Fig.15. (a)-(b) Ground orbits, attenuated backscatter profile and PBLH (symbol 'o') from the NASA
646 spaceborne lidar, CALIPSO and CATS, in the northeast US on June 12, 2017, respectively.
647

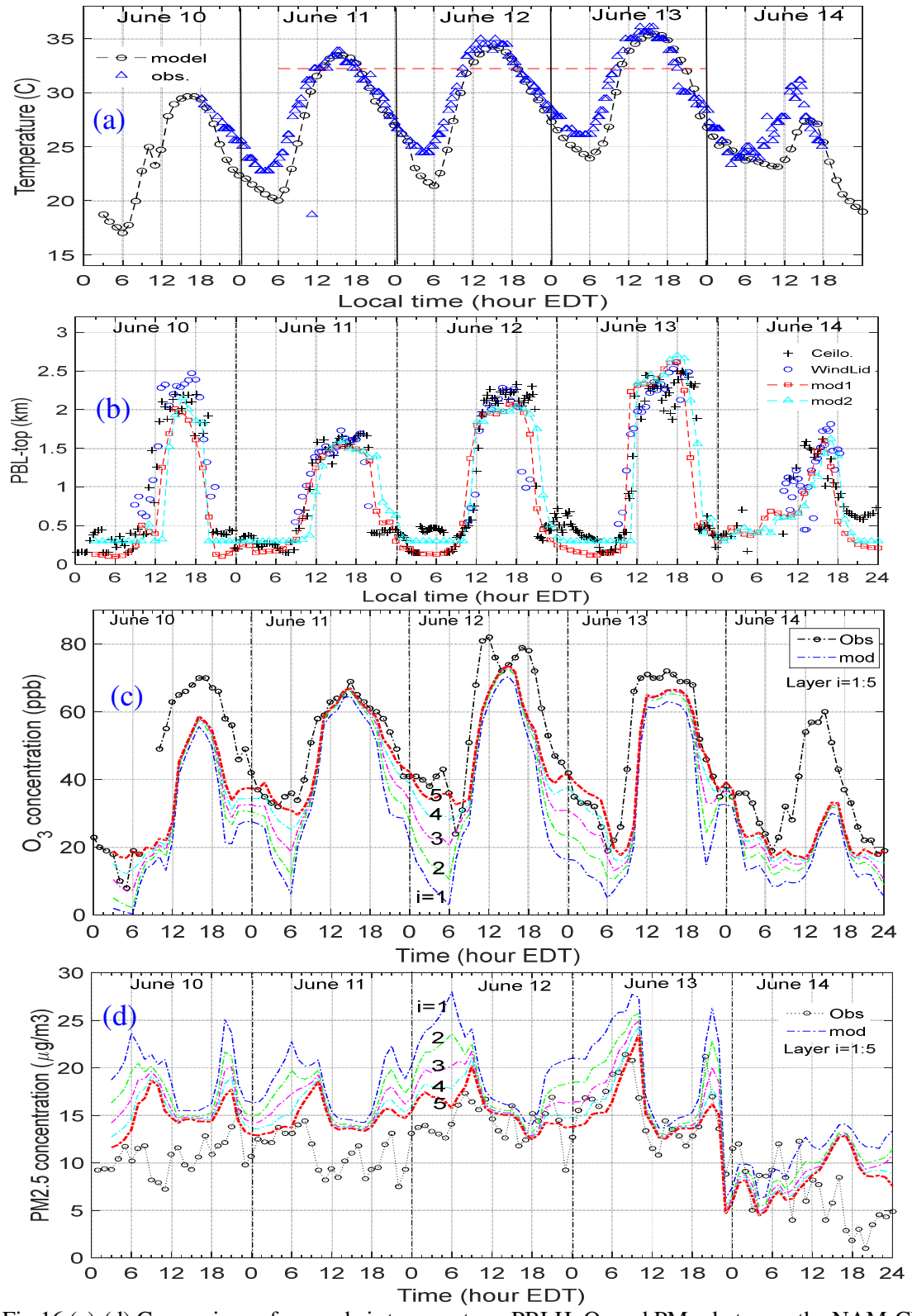

Fig.16 (a)-(d) Comparison of ground air temperature, PBLH, O_3 and $PM_{2.5}$ between the NAM-CMAQ model and observation during June 10-14, 2017 at CCNY-site. (Layer i=1~5 represents 0, 40, 80, 120 and 160 m altitude AGL. For the PBLH, mod1-mod2: different PBLH schemes.)

Regional-scale ozone (O_3) pollution is analyzed for a summer heat-wave event in New York City. Strong diurnal variation of PBL-height, O_3, PM2.5 and its species are investigated, and assess the model forecast.